The '4D-Earth-Swarm' project: CCN1

Imaging the deep Earth from rapid geomagnetic field changes

Draft Scientific Report (MS1)

a project supported by ESA

September 2022

list of partners:

- ISTerre, Grenoble, France (PI)
- ROB, Brussels, Belgium
- Univ. of Leeds, UK
- IPG, Paris, France
- DTU Space, Copenhagen, Denmark

Contents

Chapter 1

Introduction to CCN1

Nicolas Gillet, together with the 4D-Earth consortium

The objective of the main contract to understand the rapid (interannual) changes in the geomagnetic field was successfully achieved by the contractor by providing a general framework with use of Swarm observations that enables their physical understanding. This also led to the detection of Magneto-Coriolis (MC) waves for the first time. This dynamics explains sudden changes in the rate of change of the geomagnetic field (a.k.a 'jerks'), associated with pulses in the second time derivative of the field. The overarching goal of CCN1 is to contribute to a better understanding of these dynamics and to map the base state within Earth's outer core, on top of which Quasi-Geostrophic (QG) hydro-magnetic modes exist. Knowledge of the basic state within the core is expected to advance our understanding of the processes in the core generating and maintaining the Earth's dynamo. In addition, a first model of the laterally varying electrical conductivity in the region above the Core Mantle Boundary (CMB) shall be produced, using a bottom-up approach where the core dynamics is used as a source to sample the mantle conductivity. The relation between such lateral variations and the Large Low-Shear-Velocity Provinces (LLSVP) will be discussed. It should contribute to improving our understanding of the dynamical and thermo-chemical balances within the deep Earth, and thus lead to better constrain geodynamical models.

Motivations for the CCN

Sudden changes in the rate of change of the geomagnetic field (or 'jerks', see Mandea et al, 2010, for a review) have been first detected some 50 years ago in ground-based records. Over the satellite era they have been associated with pulses in the second time derivative of the field or 'secular acceleration' (Chulliat and Maus, 2014; Finlay et al, 2016). These dynamics have largely remained unexplained so far.

Prior to our project kick-off, acceleration pulses resembling those observed in geomagnetic time series had only recently been identified in geodynamo simulations approaching Earth conditions (Aubert and Finlay, 2019), thanks to a parameterization of turbulent processes (Large Eddy Simulations, or LES, see Aubert et al, 2017). They were at that stage associated in computations with one family of

quasi-geostrophic (QG, or axially invariant due to the domination of the Coriolis force) motions, non-axisymmetric QG Alfvén waves, in which inertia balances the Lorentz force in the momentum balance.

The work carried out by our consortium has allowed us to design a general framework that provides a physical understanding of rapid geomagnetic field changes. It also led to the first detection of Magneto-Coriolis (MC) waves (see Fig. 1.1) thanks to two decades of continuous magnetic monitoring from space, most recently via the Swarm mission (see Hammer et al, 2021; Finlay et al, 2020). As described below, our research domain has thus significantly evolved over the past two years.

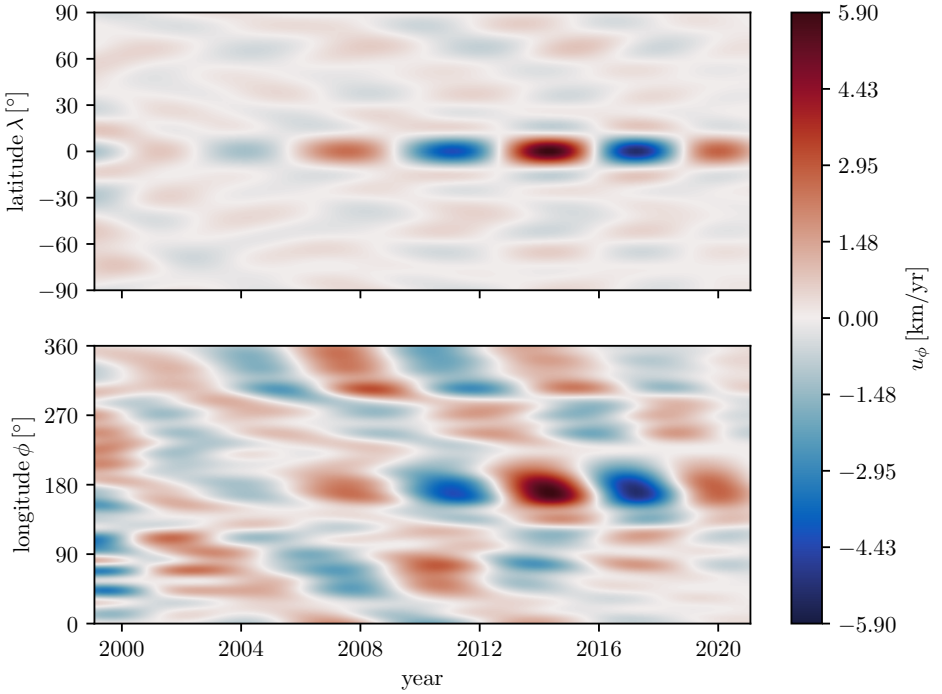

Figure 1.1: QG MC modes of period $T \sim 7$ years, detected from geomagnetic satellite data (Gillet et al, 2022). The time-latitude map for the core surface azimuthal velocity at longitude 180°E (top) shows several zero-crossings in latitude and a stronger signature towards the equator. The time-longitude diagram at the equator (bottom) illustrates a westward phase velocity of the mode, with a speed about 1500 km/yr.

First, the '71%-path' dynamo simulation run at extreme parameters (Aubert and Gillet, 2021) have shown many occurrences of magnetic acceleration events (see the catalog provided with Task E). These may be characterized depending on the relative importance of advection by the flow and wave propagation (Aubert et al, 2022). The catalog is rich in events, and a detailed analysis is required in order

to assess whether all rapid changes computed so far share the same observational and dynamical properties, and how they compare with those recorded from ground or space. The 71%-path simulation also shows QG hydromagnetic waves triggered in an ubiquitous manner, whether it be torsional (axisymmetric) Alfvén waves and QG Alfven waves on period about the Alfvén time (equivalent to $\sim$ 2 yrs in the core), or Rossby waves on shorter periods.

Meanwhile, an important breakthrough from our consortium has been the discovery of QG MC waves with interannual periods. On the large length-scales that are accessible with magnetic records ($\sim$ 800 km at the core surface), MC waves were previously believed to occur on centennial and longer periods (Hide, 1966). However, the eigenmode study by Gerick et al (2021) shows that QG MC modes do also exist on interannual periods, with a magnetic signature strongest close to the equator, as observed in satellite magnetic data (Finlay et al, 2020). This study constitutes an important theoretical and computational achievement, where two dimensional velocity perturbations in a sphere have been for the first time coupled with three-dimensional magnetic perturbations satisfying a potential field condition at the core surface.

We succeeded in detecting such a QG MC mode, with period $\sim$ 7 yr, in core surface flows inverted from satellite magnetic data (Gillet et al, 2022). These present stronger patterns in the equatorial belt (of amplitude up to 5 km/yr), and travel westward at the equator, at a phase speed $\sim$ 1500 km/yr much larger than the fluid velocity (see Fig. 1.1). This revised understanding of rapid core dynamics paves the way to a deterministic modelling of subdecadal geomagnetic field changes; a crucial part of this framework is knowledge of magnetic field within the outer core. It is the overarching goal of the current CCN to map the base state within the Earth's outer core, on top of which QG hydro-magnetic modes exist. Knowledge of the basic state withing the core will advance our understanding of the processes in the core generating and maintaining the Earth's dynamo.

So far, the main information on the field deep in the core has been obtained through the detection of torsional Alfvén waves in magnetic observations (Gillet et al, 2010). This knowledge is however restricted to a one dimensional profile, the r.m.s. of the cylindrical radial field B_s averaged over φ and z as a function of the distance s to the rotation axis (with (s, φ, z) the cylindrical coordinates). In principle, the detected QG MC modes will give access to a two dimensional map of the z-averaged r.m.s. B_s (as a function of s and φ). To more fully understand these exciting new modes and the constrains they provide we need to explore further their sensitivity to the background field with dedicated direct numerical simulations and eigenmodes studies. Furthermore, a deeper understanding of the magnetic boundary conditions relevant for the interannual dynamics may lead to improved spatial constraints on the core flow recovery. Of course, not all the magnetic signal recorded by Swarm is attached to such modes; unresolved processes also account for a significant fraction of interannual field changes (about one half according to our recent work). These two sources of signal are covariant, and properly accounting for the interplay between QG MC modes and subgrid-scale processes should

allow us to reduce uncertainties on core flows, and thus enhance the recovery of the field deep in the core.

In this quest to use Swarm observations of sub-decadal core field variations to obtain the magnetic magnetic field and fluid flow within the core, we plan to address the several issues listed below:

- upgrade and extend the geomagnetic datasets, in a manner that is suited for incorporation into core dynamics analysis tools, including adapted information on data error covariances (Task L);
- improve the `pygeodyn` core flow re-analysis tool used to isolate QG MC waves from observations, so that it better handles unresolved processes and their relation with large length-scale flows, aiming to reduce uncertainties (Task M);
- systematically detect and characterize jerks in satellite, ground observatory and geodynamo simulation data (Task N);
- image the basic state (magnetic field, velocity field and buoyancy field) within the outer core from Swarm data products, in a framework that incorporates both the statistical and dynamical information from geodynamo simulations (Task O);
- document the sensitivity of QG MC modes to the background magnetic field with an eigenmodes solver (Task P);
- extract geophysical knowledge on the core magnetic field and the lower mantle conductance in the equatorial region of the Earth's core, from the analysis of QG MC modes detected in core flow models (Task Q);
- characterize the propagation of QG MC and QG Alfvén waves in forward 3D simulations, together with the magnetic boundary conditions they satisfy, and document how these could be considered to improve the constraint on core surface flow models (Task R).

Bibliography

Aubert J, Finlay CC (2019) Geomagnetic jerks and rapid hydromagnetic waves focusing at Earth's core surface. Nature Geosci 12(5):393–398, DOI 10.1038/s41561-019-0355-1

Aubert J, Gillet N (2021) The interplay of fast waves and slow convection in geodynamo simulations nearing earth's core conditions. Geophys J Int DOI https://doi.org/10.1093/gji/ggab054

Aubert J, Gastine T, Fournier A (2017) Spherical convective dynamos in the rapidly rotating asymptotic regime. J Fluid Mech 813:558–593

Aubert J, Livermore PW, Finlay CC, Fournier A, Gillet N (2022) A taxonomy of simulated geomagnetic jerks. Geophysical Journal International 231(1):650–672

Chulliat A, Maus S (2014) Geomagnetic secular acceleration, jerks, and a localized standing wave at the core surface from 2000 to 2010. J Geophys Res: Solid Earth 119(3):1531–1543

Finlay CC, Olsen N, Kotsiaros S, Gillet N, Tøffner-Clausen L (2016) Recent geomagnetic secular variation from Swarm. Earth, Planets and Space 68(1):1–18

Finlay CC, Kloss C, Olsen N, Hammer MD, Tøffner-Clausen L, Grayver A, Kuvshinov A (2020) The chaos-7 geomagnetic field model and observed changes in the south atlantic anomaly. Earth, Planets and Space 72(1):1–31

Gerick F, Jault D, Noir J (2021) Fast quasi-geostrophic magneto-coriolis modes in the earth's core. Geophys Res Lett p 2020GL090803

Gillet N, Jault D, Canet E, Fournier A (2010) Fast torsional waves and strong magnetic field within the Earth's core. Nature 465(7294):74

Gillet N, Gerick F, Jault D, Schwaiger T, Aubert J, Istas M (2022) Satellite magnetic data reveal interannual waves in earth,Äôs core. Proceedings of the National Academy of Sciences 119(13):e2115258,119

Hammer MD, Cox GA, Brown WJ, Beggan CD, Finlay CC (2021) Geomagnetic virtual observatories: monitoring geomagnetic secular variation with the swarm satellites. Earth, Planets and Space 73(1):1–22

Hide R (1966) Free hydromagnetic oscillations of the earth's core and the theory of the geomagnetic secular variation. Phil Trans R Soc London Series A, Mathematical and Physical Sciences 259(1107):615–647

Mandea M, Holme R, Pais A, Pinheiro K, Jackson A, Verbanac G (2010) Geomagnetic jerks: rapid core field variations and core dynamics. Space science reviews 155(1):147–175

Chapter 2

Descriptions of the datasets

2.1 Updated geomagnetic datasets, and data error covariance matrices (preliminary release)

4DEarth_Swarm_Core ESA project deliverable CCN1 D-L.1

Chris Finlay, Magnus Hammer, Clemens Kloss and Nils Olsen
DTU Space, Technical University of Denmark

For the description of the data formats, we refer to Section § 2.1 (deliverable D-B.1) of the final version of the Scientific Report (before the start of CCN1).

2.1.1 updated GVO Datasets

The updated GVO series used in the submitted article by Istas et al. (including the new 12-monthly averaged versions of the datasets) as well Grace GVOs have been archived at the usual GVO site:

`http://www.spacecenter.dk/files/magnetic-models/GVO/`

- Swarm (including the official versions produced by BGS):

`http://www.spacecenter.dk/files/magnetic-models/GVO/GVO_data_SWARM.zip`

- CHAMP:

`http://www.spacecenter.dk/files/magnetic-models/GVO/GVO_data_CHAMP.zip`

- Oersted:

`http://www.spacecenter.dk/files/magnetic-models/GVO/GVO_data_OERSTED.zip`

- Cryosat-2:

`http://www.spacecenter.dk/files/magnetic-models/GVO/GVO_data_CRYOSAT2.zip`

- Composite series:

`http://www.spacecenter.dk/files/magnetic-models/GVO/GVO_data_Composite.zip`

- GRACE:

`http://www.spacecenter.dk/files/magnetic-models/GVO/GVO_data_GRACE.zip`

Note the GVO zip folder locations for latest versions remain the same, but files are updated, older versions moved into an archived version at :

`http://www.spacecenter.dk/files/magnetic-models/GVO/archive/version_0201_March22/`

Work has been carried out on full data error covariance matrices, including off-diagonal elements for the 4 montly GVOs. Different approaches going beyond the standard calculation of empirical covariance matrices have explored and compared, in particular (i) Graphical Lasso (Friedman et al, 2008) for promoting sparse

covariance matrices, (ii) Optimal Covariance shrinkage (Ledoit and Wolf, 2004), and (iii) Averaging covariances over QD latitude zones. Preliminary results show encouraging performance, in particular from approach (ii).

2.1.2 Ground Observatory (GO) series

The revised monthly mean (RMM) data series was updated in September 2022 using data from the BGS AUX_OBS database up to June 2022. It will be available in cdf form before the end of September 2022 at:

`http://www.spacecenter.dk/files/magnetic-models/GO/`

2.1.3 CHAOS field model

The CHAOS field model was updated in July 2022 to version 7.11 using Swarm data preliminary release 0602, using data up to end of May 2022. This model is available at:

`http://www.spacecenter.dk/files/magnetic-models/CHAOS-7/`

Work on a further update to version 7.12 using Swarm 0602 data to end of August 2022 is underway and it and the associated datasets will be available at the above webpage by the end of September 2022.

The CHAOS field modelling software has been updated to allow for along-track correlated errors in the satellite data. This has been implemented via an eigenanalysis method and tested in simple field modelling experiments using a simple exponential covariance function.

The resolution matrix from the CHAOS field model has been investigated and experiments carried out to explore whether it can help to better informing geodynamicists as to what features of the core field and its time derivatives are adequately resolved. A similar approach has proved useful in seismic tomography.

Bibliography

Friedman J, Hastie T, Tibshirani R (2008) Sparse inverse covariance estimation with the graphical lasso. Biostatistics 9(3):432–441

Ledoit O, Wolf M (2004) A well-conditioned estimator for large-dimensional covariance matrices. Journal of multivariate analysis 88(2):365–411

2.2 An ensemble of 3D base states for Earth's core dynamics at epoch 2000 determined by geomagnetic data assimilation in a numerical geodynamo model

4DEarth_Swarm_Core ESA project deliverable CCN1 D-O.1

J. Aubert
IPG Paris

2.2.1 General description

This document refers to publicly available output data from a sequential framework that assimilates geomagnetic data into a numerical model of the geodynamo. The framework estimates the internal, three-dimensional state of Earth's inner and outer core according to the model, along a temporal trajectory punctuated by analysis points where the geomagnetic data at the core surface are combined with the internal dynamics of a background model, following an Kalman filtering strategy (see Aubert, 2015).

Mathematical models of the geomagnetic field (sets of spherical harmonic coefficients describing the core surface magnetic field and its rate-of-change, both up to spherical harmonic degree and order 13), are used as input data to the framework from epoch 1840 to epoch 2000. The geomagnetic field models COV-OBS (Gillet et al, 2013) is used to spin up the assimilation by performing 13 discrete analyses between epochs 1840 and 1990, after which a 14th analysis performed in epoch 2000 using the field model CHAOS-7-x9 (Finlay et al, 2020). While performing the analyses, the background geodynamo model is progressively advanced along a "path to Earth's core" in numerical simulation parameter space (Aubert et al, 2017), and reaches 43% along this path at epoch 2000.

The output data supplied here corresponds to the final base state at epoch 2000, that is suitable for subsequent theoretical and numerical work of the rapid dynamics that sets up on top of this base state throughout the satellite era 2000-2022. This state is not unique, because the variability of parts that are hidden to observation need to be estimated in a statistical way. What is supplied here is therefore an ensemble of 42 three-dimensional base states for the Earth's core at epoch 2000, that attempt to respect the statics (core surface magnetic field morphology) and kinematics (core surface magnetic field rate-of-change, associated core surface flow, leading order "QG-MAC" force balance) while adhering to the dynamical constraints enforced at this position along the parameter space path, and sampling the variability of hidden quantities.

2.2.2 Data format and description

The file format is MATLAB `.mat` in version 7.3 i.e. HDF5 compliant. The output uses a discretisation in physical space along the radial direction, while the lateral directions are described in a spectral way on a basis of spherical harmonics.

The file `Gauss_state.mat` contains:

- The radius vector `r(1:nr)` with `nr`=140, the number of radial grid points of the discretisation, and `ng`=14, the position of the inner-core boundary in the array `r(1:nr)`. The physical unit of `r` is km.
- The arrays `Bpnm(1:42,1:961,1:nr)` and `Btnm(1:42,1:961,1:nr)` respectively describing the 961 poloidal and toroidal spherical harmonic coefficients of the magnetic field, over the radial grid defined by `r(1:nr)` (hence comprising the electrically conducting inner core), and for the 42 members of the ensemble. The physical unit of `Bpnm` is T.km and that of `Btnm` is T.
- The arrays `Vpnm(1:42,1:961,1:nr-ng+1)` and `Vtnm(1:42,1:961,1:nr-ng+1)` respectively describing the 961 poloidal and toroidal spherical harmonic coefficients of the velocity field, over the radial grid defined by `r(ng:nr)` (hence excluding the inner core), and for the 42 members of the ensemble. The physical unit of `Vpnm` is $\mathrm{km}^2/\mathrm{yr}$ and that of `Vtnm` is km/yr.
- The array `Cnm(1:42,1:961,1:nr-ng+1)` describing the 961 poloidal and toroidal spherical harmonic coefficients of the density anomaly field, over the radial grid defined by `r(ng:nr)` (hence excluding the inner core), and for the 42 members of the ensemble. The physical unit of `Cnm` is kg/m^3.

Choosing a spherical coordinate frame with radius r, colatitude θ and the Greenwich-centered longitude φ, The poloidal-toroidal decomposition is adopted for the velocity field $\mathbf{u}$ and the magnetic field $\mathbf{B}$, such that:

$$\mathbf{u} = \nabla \times (Vt(r,\theta,\varphi)\mathbf{r}) + \nabla \times \nabla \times (Vp(r,\theta,\varphi)\mathbf{r}),$$
$$\mathbf{B} = \nabla \times (Bt(r,\theta,\varphi)\mathbf{r}) + \nabla \times \nabla \times (Bp(r,\theta,\varphi)\mathbf{r}).$$

Note that $\mathbf{r} = r\mathbf{e}_r$ is the **radius vector**, and **not** the radial unit vector $\mathbf{e}_r$. The density anomaly $C(r,\theta,\varphi)$ does not need such an expansion as it is a scalar field.

The scalar fields $X = Vt, Vp, Bt, Bp, C$ describing the velocity, magnetic vector fields as well as the scalar density anomaly field are supplied as real spherical harmonic coefficients $c_\ell^m(r)$ and $s_\ell^m(r)$ following

$$X(r,\theta,\varphi) = \sum_{\ell=0}^{30} \sum_{m=0}^{\ell} \left[c_\ell^m(r) \cos m\varphi + s_\ell^m(r) \sin m\varphi \right] P_\ell^m(\cos\theta)$$

Here P_ℓ^m is the Schmidt-seminormalised Legendre function of degree ℓ and order m. The base state is therefore supplied up to spherical harmonic degree and order

$\ell_{\max} = m_{\max} = 30$. For each ensemble member labelled i, and in the case where the inner core is included (i.e. the case of magnetic field coefficients), the ordering of radially discretized coefficients into MATLAB arrays follows:

$$\begin{aligned}
\texttt{Xnm}(i, 1, [1 : \texttt{nr}]) &= c_0^0(\texttt{r}[1 : \texttt{nr}]) \\
\texttt{Xnm}(i, 2, [1 : \texttt{nr}]) &= c_1^0(\texttt{r}[1 : \texttt{nr}]) \\
\texttt{Xnm}(i, 3, [1 : \texttt{nr}]) &= c_1^1(\texttt{r}[1 : \texttt{nr}]) \\
\texttt{Xnm}(i, 4, [1 : \texttt{nr}]) &= s_1^1(\texttt{r}[1 : \texttt{nr}]) \\
\texttt{Xnm}(i, 5, [1 : \texttt{nr}]) &= c_2^0(\texttt{r}[1 : \texttt{nr}]) \\
\texttt{Xnm}(i, 6, [1 : \texttt{nr}]) &= c_2^1(\texttt{r}[1 : \texttt{nr}]) \\
\texttt{Xnm}(i, 7, [1 : \texttt{nr}]) &= s_2^1(\texttt{r}[1 : \texttt{nr}]) \\
\texttt{Xnm}(i, 8, [1 : \texttt{nr}]) &= c_2^2(\texttt{r}[1 : \texttt{nr}]) \\
\texttt{Xnm}(i, 9, [1 : \texttt{nr}]) &= s_2^2(\texttt{r}[1 : \texttt{nr}]) \\
&\ldots \\
\texttt{Xnm}(i, 960, [1 : \texttt{nr}]) &= c_{30}^{30}(\texttt{r}[1 : \texttt{nr}]) \\
\texttt{Xnm}(i, 961, [1 : \texttt{nr}]) &= s_{30}^{30}(\texttt{r}[1 : \texttt{nr}])
\end{aligned}$$

In the case where the inner core is excluded (velocity and density anomaly field coefficients) these relationships write e.g.:

$$\texttt{Xnm}(i, 1, [1 : \texttt{nr} - \texttt{ng} + 1]) = c_0^0(\texttt{r}[\texttt{ng} : \texttt{nr}])$$

Note that the sinus coefficients corresponding to $m = 0$ are not stored as they vanish identically. Note also that unlike previous deliverables of this project, the coefficient c_0^0 is supplied because it is non-zero for the density anomaly field (but it is otherwise vanishing for all other solenoidal fields).

2.2.3 Graphics for validation

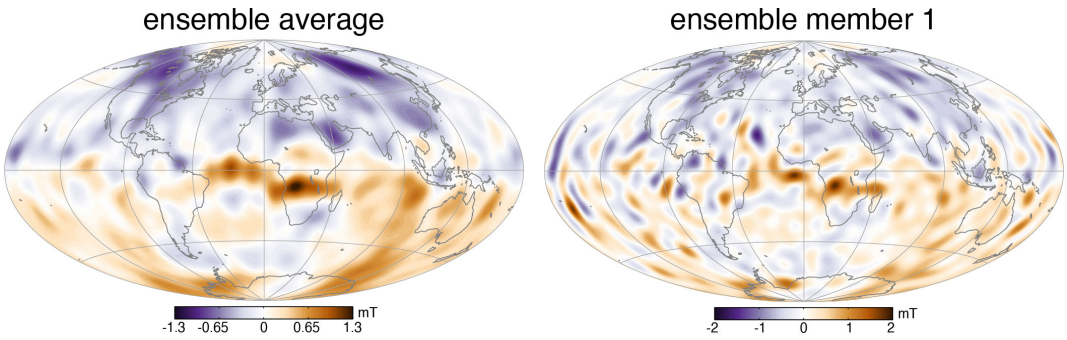

Figure 2.1: Hammer projection of the radial magnetic field at the external boundary (radial level `nr`=140) of the model, for the ensemble average (left) and first member of the ensemble (right).

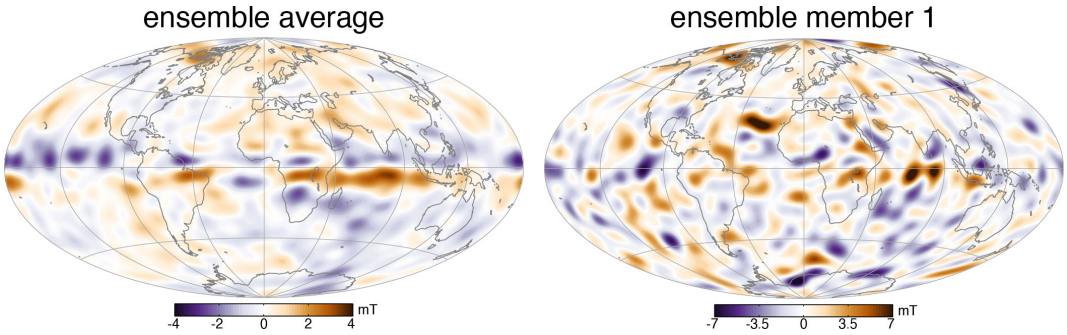

Figure 2.2: Hammer projection of the azimuthal magnetic field at the radial level `ir` = 121, corresponding to about 102 km below the core surface, for the ensemble average (left) and first member of the ensemble (right).

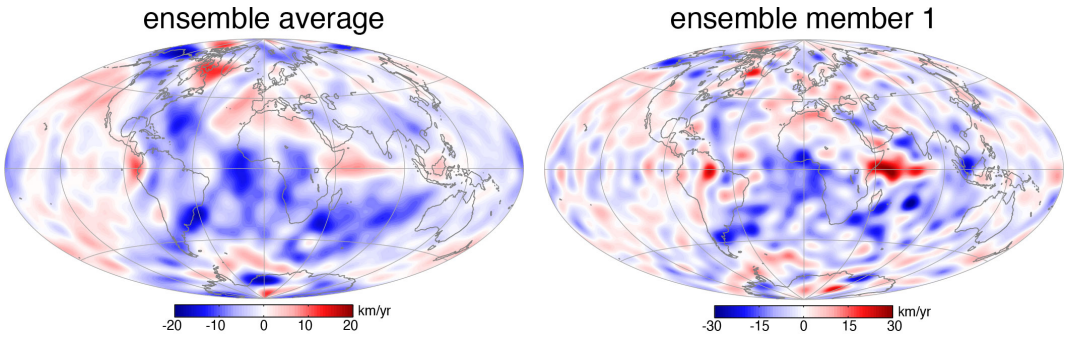

Figure 2.3: Hammer projection of the azimuthal velocity field at the external boundary (radial level `nr`=140) of the model, for the ensemble average (left) and first member of the ensemble (right).

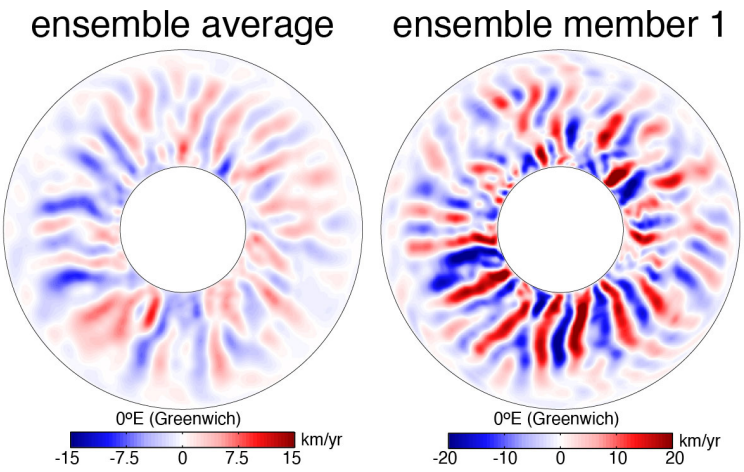

Figure 2.4: Radial velocity field in the equatorial plane, for the ensemble average (left) and first member of the ensemble (right).

Bibliography

Aubert J (2015) Geomagnetic forecasts driven by thermal wind dynamics in the Earth's core. Geophys J Int 203(3):1738–1751

Aubert J, Gastine T, Fournier A (2017) Spherical convective dynamos in the rapidly rotating asymptotic regime. J Fluid Mech 813:558–593

Finlay CC, Kloss C, Olsen N, Hammer MD, Tøffner-Clausen L, Grayver A, Kuvshinov A (2020) The chaos-7 geomagnetic field model and observed changes in the south atlantic anomaly. Earth, Planets and Space 72(1):1–31

Gillet N, Jault D, Finlay CC, Olsen N (2013) Stochastic modeling of the Earth's magnetic field: Inversion for covariances over the observatory era. Geochem Geophys Geosyst 14(4):766–786, DOI {10.1002/ggge.20041}

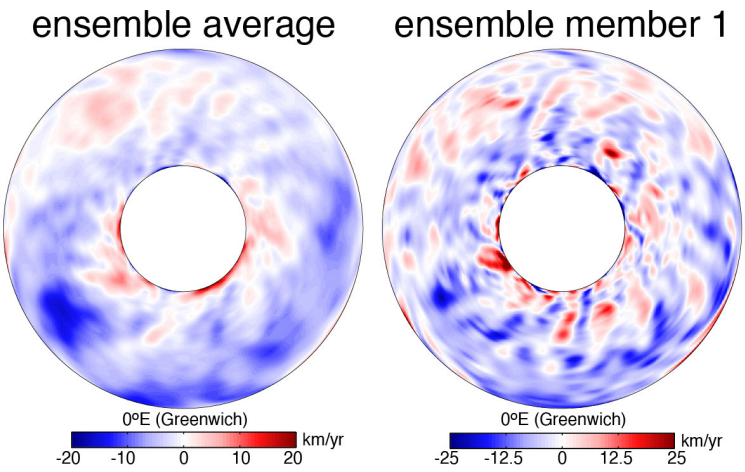

Figure 2.5: Azimuthal velocity field in the equatorial plane, for the ensemble average (left) and first member of the ensemble (right).

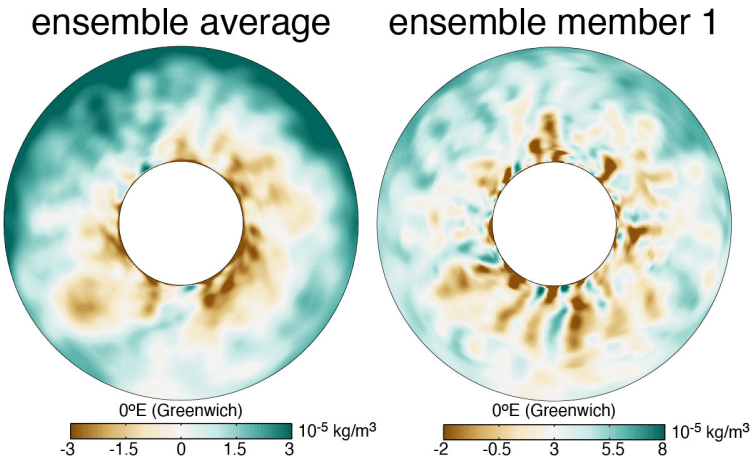

Figure 2.6: Density anomaly field in the equatorial plane, for the ensemble average (left) and first member of the ensemble (right).

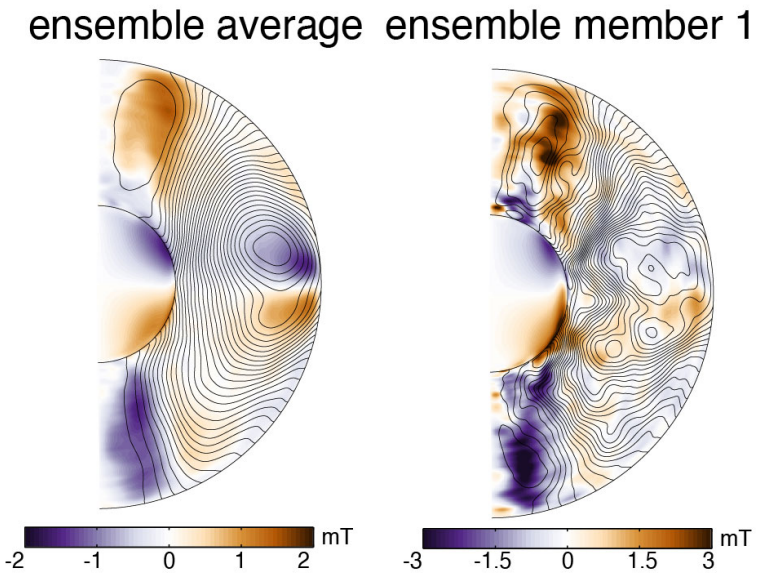

Figure 2.7: Meridional cut of the axisymmetrically-averaged azimuthal magnetic field, for the ensemble average (left) and first member of the ensemble (right). Overplotted are also the field lines corresponding to the azimuthally averaged poloidal magnetic field.

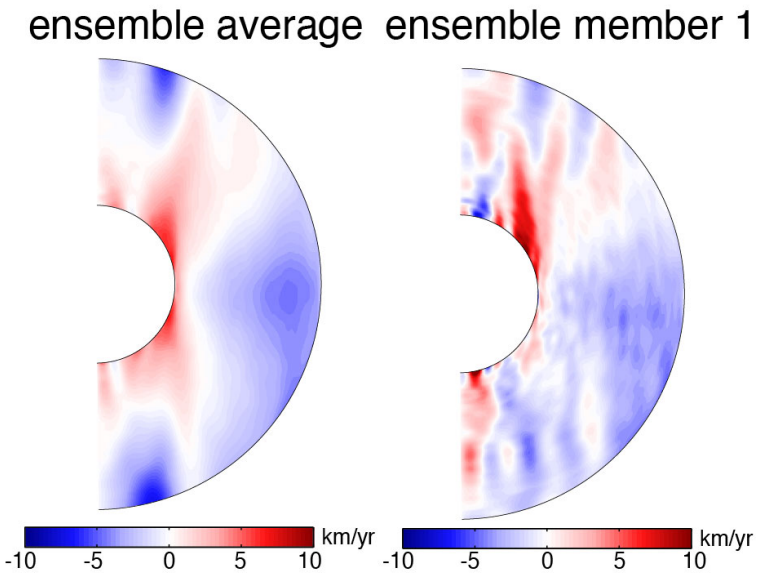

Figure 2.8: Meridional cut of the axisymmetrically-averaged azimuthal velocity field, for the ensemble average (left) and first member of the ensemble (right).

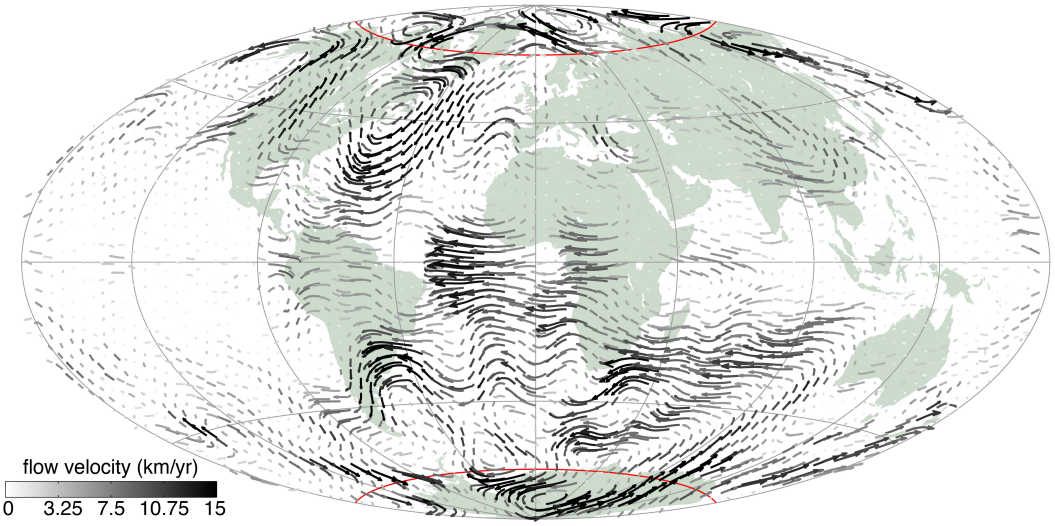

Figure 2.9: Quiver plot of the core surface velocity field for the ensemble average, in Hammer equatorial view, with the arrow greyscale representing the flow amplitude.

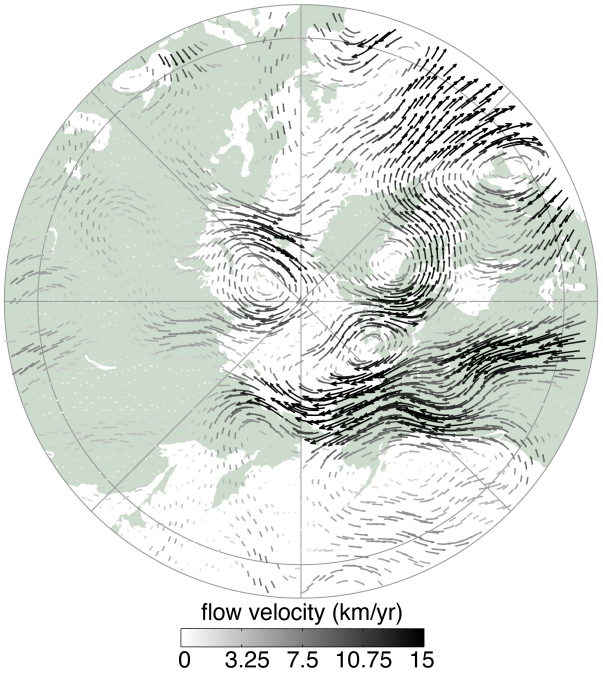

Figure 2.10: Quiver plot of the core surface velocity field for the ensemble average, in North polar view, with the arrow greyscale representing the flow amplitude.